

The 3rd African Conference on Fundamental and Applied Physics  
(ACP2023)  
[exauce.bokamba@umng.cg](mailto:exauce.bokamba@umng.cg)

## STUDY OF SPECTRA OF HF VI

E. Bokamba Motoumba<sup>a,\*</sup>, S. Enzonga Yoca<sup>a,b</sup>, P. Quinet<sup>c,d</sup>, P. Palmeri<sup>c</sup>

<sup>a</sup> Faculté des Sciences et Techniques, Université Marien Nguabi, Brazzaville, Congo

<sup>b</sup> Conseil Africain et Malgache pour l'Enseignement Supérieur – CAMES, Ouagadougou, Burkina Faso

<sup>c</sup> Physique Atomique et Astrophysique, Université de Mons – UMONS, Mons, B 7000, Belgium  
<sup>d</sup> IPNAS, Université de Liège, Liège, B 4000, Belgium

ACP2023, George, South Africa, September 25, 2023

# Plan

- 1 Introduction
- 2 Methods used and calculations
- 3 Results
- 4 Conclusion

# Plan

- 1 Introduction
- 2 Methods used and calculations
- 3 Results
- 4 Conclusion

# Plan

- 1 Introduction
- 2 Methods used and calculations
- 3 Results
- 4 Conclusion

# INTRODUCTION

5

Hafnium ( $Z = 72$ ) is an element that could be employed in plasma-facing materials in Tokamaks [1, 2] and is also produced in neutron-induced transmutation of tungsten ( $Z = 74$ ) and its alloys that will compose the **divertors in these fusion reactors** [3]. As a consequence, their sputtering may generate ionic impurities of all possible charge states in the deuterium-tritium plasma. These impurities could contribute to radiation losses in controlled nuclear fusion devices. The radiative properties of these ions have therefore potential important applications in this field.

**Opacity calculations**

**Cosmochronology**

# INTRODUCTION

6

To our knowledge, few studies have been dedicated to the Hf VI spectrum. In 2012, Ryabtsev *et al.* [4] classified the Hf VI  $5s^25p^64f^{13} - 5s^25p^54f^{13}6s$  transitions in spectra recorded in the ultraviolet (UV) range 145 – 350 Å using a low-inductive vacuum spark source and a grazing-incidence vacuum spectrograph. A few years later, they analysed the UV spectra recorded by two high-resolution vacuum spectrographs, one in the region 190 – 350 Å using the Institute of Spectroscopy Troisk grating spectrograph and the other in the spectral range 300 – 500 Å using the Meudon Observatory grating spectrograph [5]. They classified 185 Hf VI lines as transitions from the excited even-parity configurations  $5s^25p^64f^{12}5d$ ,  $5s^25p^64f^{12}6d$ ,  $5s^25p^54f^{13}5d$ ,  $5s^25p^54f^{13}6s$ ,  $5s^25p^44f^{14}5d$ ,  $5s^25p^44f^{14}6s$  and  $5s5p^64f^{14}$  to the two low-lying odd-parity configurations  $5s^25p^64f^{13}$  and  $5s^25p^54f^{14}$ , and found 137 even-parity fine-structure levels.

# INTRODUCTION

7

Following our previous work on erbium-like Lu IV, Hf V and Ta VI [6], a multiplatform approach has been adopted to determine the transition probabilities of electric dipole (E1) lines in Hf VI and evaluate their accuracy. It consisted of using the semi-empirical Hartree–Fock with relativistic corrections method (HFR) [7] and the *ab initio* multiconfiguration Dirac–Hartree–Fock with subsequent relativistic configuration-interaction method (MCDHF–RCI) [8].

# Methods Used and Calculations

In order to determine the radiative parameters in Hf VI, we have performed three independent calculations. One was based on the semi-empirical HFR method [7] that relies on the availability of experimental energy levels while the other two were purely *ab initio* and were both based on the MCDHF method [8]. In the subsequent subsections, we provide the details of three atomic structure computations carried out in this work.



# Methods Used and Calculations

9

## The Semi-Empirical HFR Method

Based on Schrodinger equation

Multiconfiguration approach

One-body relativistic corrections (spin-orbit, mass-velocity, Darwin)

Semi-empirical optimisation of radial parameters

# Methods Used and Calculations

10

## Radial parameters (in $\text{cm}^{-1}$ ) adopted in the HFR model

heightConfiguration	Parameter	<i>Ab initio</i>	Fitted	Unc.	Ratio	Remark <sup>a</sup>
Odd Parity						
4f <sup>13</sup>	$E_{av}$	9 379	9 304	0	/	
	$\zeta_{4f}$	3 910	3 860	0	0.99	
5p <sup>5</sup> 4f <sup>14</sup>	$E_{av}$	144 722	122 947	0	/	
	$\zeta_{5p}$	44 366	43 377	0	0.98	
5p <sup>4</sup> 4f <sup>14</sup> 6p	$E_{av}$	603 097	/	/	/	F
5p <sup>4</sup> 4f <sup>14</sup> 7p	$E_{av}$	747 678	/	/	/	F
5p <sup>4</sup> 4f <sup>14</sup> 5f	$E_{av}$	698 581	/	/	/	F
5p <sup>4</sup> 4f <sup>14</sup> 6f	$E_{av}$	790 741	/	/	/	F
5p <sup>4</sup> 4f <sup>14</sup> 7f	$E_{av}$	839 774	/	/	/	F
5s5p <sup>5</sup> 4f <sup>14</sup> 5d	$E_{av}$	750 601	/	/	/	F
5s5p <sup>5</sup> 4f <sup>14</sup> 6s	$E_{av}$	821 762	/	/	/	F
4f <sup>12</sup> 6p	$E_{av}$	398 203	/	/	/	F
4f <sup>12</sup> 7p	$E_{av}$	547 186	/	/	/	F
4f <sup>12</sup> 5f	$E_{av}$	497 446	/	/	/	F
4f <sup>12</sup> 6f	$E_{av}$	591 157	/	/	/	F
4f <sup>12</sup> 7f	$E_{av}$	641 024	/	/	/	F

# Methods Used and Calculations

11

## Radial parameters (in $\text{cm}^{-1}$ ) adopted in the HFR model

Configuration	Parameter	<i>Ab initio</i>	Fitted	Unc.	Ratio	Remark <sup>d</sup>
Even Parity						
4f <sup>12</sup> 5d	$E_{av}$	242 100	253 718	136	/	
	$F^2(4f4f)$	169 487	134 724	1 175	0.80	R1
	$F^4(4f4f)$	107 320	98 429	3 222	0.92	R2
	$F^6(4f4f)$	77 495	74 509	3 299	0.96	R3
	$\alpha$	/	14.5	15	/	R4
	$\beta$	/	-309	678	/	R5
	$\gamma$	/	-541	760	/	R6
	$\zeta_{4f}$	4 084	3 936	35	0.96	R7
	$\zeta_{5d}$	3 341	3 283	83	0.98	R8
	$F^2(4f5d)$	41 113	33 380	965	0.81	R9
	$F^4(4f5d)$	19 700	15 995	462	0.81	R9
	$G^1(4f5d)$	15 084	12 207	431	0.81	R10
	$G^3(4f5d)$	13 666	11 059	391	0.81	R10
	$G^5(4f5d)$	10 797	8 738	309	0.81	R10
4f <sup>12</sup> 6d	$E_{av}$	497 311	508 595	123	/	
	$F^2(4f4f)$	170 072	135 196	1 179	0.80	R1
	$F^4(4f4f)$	107 723	98 801	3 234	0.92	R2

# Methods Used and Calculations

12

## Radial parameters (in $\text{cm}^{-1}$ ) adopted in the HFR model

Configuration	Parameter	<i>Ab initio</i>	Fitted	Unc.	Ratio	Remark <sup>a</sup>
	$F^6(4f4f)$	77 795	74 801	3 312	0.96	R3
	$\alpha$	/	14.5	15	/	R4
	$\beta$	/	-309	678	/	R5
	$\gamma$	/	-541	760	/	R6
	$\zeta_{4f}$	4 096	3 949	35	0.96	R7
	$\zeta_{6d}$	880	865	22	0.98	R8
	$F^2(4f6d)$	10 244	8 317	240	0.81	R9
	$F^4(4f6d)$	4 465	3 626	105	0.81	R9
	$G^1(4f6d)$	3 012	2 438	86	0.81	R10
	$G^3(4f6d)$	2 999	2 444	86	0.82	R10
	$G^5(4f6d)$	2 450	1 997	70	0.82	R10
$4f^{12}7d$	$E_{av}$	592 905	/	/	/	F
$4f^{12}6s$	$E_{av}$	323 531	/	/	/	F
$4f^{12}7s$	$E_{av}$	514 961	/	/	/	F

# Methods Used and Calculations

13

## Radial parameters (in $\text{cm}^{-1}$ ) adopted in the HFR model

Configuration	Parameter	<i>Ab initio</i>	Fitted	Unc.	Ratio	Remark <sup>a</sup>
$5p^5 4f^{13} 5d$	$E_{av}$	335 112	335 399	139	/	
	$\zeta_{5p}$	46 768	46 349	106	0.99	R11
	$\zeta_{4f}$	3 926	3 810	34	0.97	R7
	$\zeta_{5d}$	3 127	3 071	77	0.98	R8
	$F^2(4f5p)$	65 743	48 272	1 282	0.73	R12
	$F^2(4f5d)$	40 193	32 206	931	0.80	R9
	$F^4(4f5d)$	19 319	15 479	447	0.80	R9
	$F^2(5p5d)$	72 028	61 487	1 461	0.85	R13
	$G^2(4f5p)$	29 055	22 939	1 068	0.79	R14
	$G^4(4f5p)$	23 478	18 535	863	0.79	R14
	$G^1(4f5d)$	15 377	12 155	429	0.79	R10
	$G^3(4f5d)$	13 668	10 804	382	0.79	R10
	$G^5(4f5d)$	10 729	8 481	300	0.79	R10
	$G^1(5p5d)$	86 223	60 294	460	0.70	R15
$G^3(5p5d)$	53 937	37 719	288	0.70	R15	
$5p^5 4f^{13} 6d$	$E_{av}$	580 255	/	/	/	F
$5p^5 4f^{13} 7d$	$E_{av}$	674 301	/	/	/	F
$5p^5 4f^{13} 6s$	$E_{av}$	480 664	406 406	116	/	
	$\zeta_{5p}$	47 755	47 327	108	0.99	R11
	$\zeta_{4f}$	3 934	3 819	34	0.97	R7

# Methods Used and Calculations

14

## Radial parameters (in $\text{cm}^{-1}$ ) adopted in the HFR model

Configuration	Parameter	<i>Ab initio</i>	Fitted	Unc.	Ratio	Remark <sup>a</sup>
	$F^2(4f5p)$	66 454	48 795	1 295	0.73	R12
	$G^2(4f5p)$	29 289	23 122	1 076	0.79	R14
	$G^4(4f5p)$	23 728	18 732	872	0.79	R14
	$G^3(4f6s)$	4 660	4 387	1 821	0.94	
	$G^1(5p6s)$	9 597	9 004	681	0.94	R16
$5p^5 4f^{13} 6s$	$E_{av}$	408 162	/	/	/	F
$5p^5 4f^{13} 7s$	$E_{av}$	596 817	/	/	/	F
$5s 5p^6 4f^{14}$	$E_{av}$	441 391	/	/	/	F
$5s 5p^6 4f^{13} 6p$	$E_{av}$	894 190	/	/	/	F
$5s 5p^6 4f^{13} 5f$	$E_{av}$	989 789	/	/	/	F
$5p^4 4f^{14} 5d$	$E_{av}$	464 345	455 999	252	/	
	$F^2(5p5p)$	89 426	71 236	1 793	0.80	R17
	$\zeta_{5p}$	45 099	44 693	102	0.99	R11
	$\zeta_{5d}$	2 935	2 882	72	0.98	R8
	$F^2(5p5d)$	70 482	60 166	1 429	0.85	R13
	$G^1(5p5d)$	84 039	58 764	448	0.70	R15
	$G^3(5p5d)$	52 546	36 743	280	0.70	R15
$5p^4 4f^{14} 6d$	$E_{av}$	700 115	/	/	/	F
$5p^4 4f^{14} 7d$	$E_{av}$	792 791	/	/	/	F

# Methods Used and Calculations

15

## Radial parameters (in $\text{cm}^{-1}$ ) adopted in the HFR model

Configuration	Parameter	<i>Ab initio</i>	Fitted	Unc.	Ratio	Remark <sup>a</sup>
$5p^4 4f^{14} 6s$	$E_{av}$	529 824	518 642	264	/	
	$F^2(5p5p)$	90 140	71 804	1 807	0.80	R17
	$\zeta_{5p}$	46 044	45 631	104	0.99	R11
	$G^1(5p6s)$	9 618	9 023	683	0.94	R16
$5p^4 4f^{14} 7s$ $4f^{12} 5d - 5p^5 4f^{13} 5d$	$E_{av}$	715 751	/	/	/	F
	$R^2(5p4f, 4f4f)$	-9 453	-7 326	462	0.78	R18
	$R^4(5p4f, 4f4f)$	-2 559	-1 983	125	0.78	R18
	$R^2(5p5p, 4f5p)$	-39 662	-30 737	1 936	0.78	R18
	$R^2(5p5d, 4f5d)$	-29 360	-22 753	1 433	0.78	R18
	$R^4(5p5d, 4f5d)$	-18 828	-14 591	919	0.78	R18
	$R^1(5p5d, 5d4f)$	-26 380	-20 444	1 288	0.78	R18
	$R^3(5p5d, 5d4f)$	-19 128	-14 824	934	0.78	R18
$4f^{12} 5d - 5p^4 4f^{14} 5d$	$R^2(5p5p, 4f4f)$	29 861	29 525	890	0.99	R19
	$R^4(5p5p, 4f4f)$	23 915	23 646	676	0.99	R19
$5p^5 4f^{13} 5d - 5p^4 4f^{14} 5d$	$R^2(4f5p, 4f4f)$	-11 441	-5 614	624	0.49	R20
	$R^4(4f5p, 4f4f)$	-3 959	-1 943	216	0.49	R20
	$R^2(5p5p, 4f5p)$	-40 669	-19 957	2 220	0.49	R20
	$R^2(5p5d, 4f5d)$	-29 854	-14 650	1 629	0.49	R20
	$R^4(5p5d, 4f5d)$	-19 073	-9 360	1 041	0.49	R20
	$R^1(5p5d, 5d4f)$	-27 153	-13 325	1 482	0.49	R20
	$R^3(5p5d, 5d4f)$	-19 461	-9 550	1 062	0.49	R20

<sup>a</sup> Parameters marked with the same  $Rn$  (with  $n = 1 - 20$ ) have their variation linked together by their corresponding HFR ratios keeping fixed during the fitting procedure. Those marked with F have been fixed.

# Methods Used and Calculations

16

## The Ab initio MCDHF Method

Based on Dirac's equation

Multiconfiguration approach

Fully Relativistic + QED corrections

Purely ab initio



# Methods Used and Calculations

17

## The Ab initio MCDHF Method

The present *ab initio* calculations were focused on the electric dipole transitions starting from the two odd-parity levels with symmetries  $J^{\Pi} = 5/2^{\circ}, 7/2^{\circ}$  of the ground configuration, *i.e.*  $5s^25p^64f^{13}$ , and from the two excited odd-parity levels with symmetries  $J^{\Pi} = 1/2^{\circ}, 3/2^{\circ}$  belonging to the configuration  $5s^25p^54f^{14}$  and ending on the 137 even-parity levels with symmetries  $J^{\Pi} = 1/2^e - 9/2^e$  belonging to the configurations  $5s^25p^64f^{12}(5d, 6d)$ ,  $5s^25p^54f^{13}(5d, 6s)$ ,  $5s^25p^44f^{14}(5d, 6s)$  and  $5s5p^64f^{14}$  classified by Ryabtsev *et al.* [5].

2 models used for CSF expansions MCDHF-RCI-A and MCDHF-RCI-B

## The Ab initio MCDHF Method

In the first MCDHF-RCI calculation, the following spectroscopic configurations were considered in the MR:  $5s^25p^64f^{13}$ ,  $5s^25p^54f^{14}$  with symmetries  $J^\Pi = 1/2^o - 7/2^o$ ;  $5s^25p^64f^{12}(5d, 6d)$ ,  $5s^25p^54f^{13}(5d, 6s)$ ,  $5s^25p^44f^{14}(5d, 6s)$  and  $5s5p^64f^{14}$  with symmetries  $J^\Pi = 1/2^e - 9/2^e$ . The AS was  $6s6p6d6f$ . All single and double electron excitations from the occupied orbitals except the core subshells up to the 4d orbital which were kept closed were considered to build a basis of 4 126 144 CSFs. The latter has been further reduced to 3 545 069 CSFs by deleting the ones that weakly interact with the CSFs of the MR through the Dirac-Coulomb-Breit (DCB) Hamiltonian [8]. The orbitals were obtained in separate Dirac-Hartree-Fock Extended Average Level (EAL) [8, 9] self-consistent-field (SCF) optimizations on a single configuration as follows: all the core orbitals, meaning 1s to 4d, along with the 5s, 5p and 4f valence orbitals were optimized on the ground configuration  $5s^25p^64f^{13}$ ; for the others, each  $n\ell$  orbital of the AS were optimized on a configuration of the corresponding type  $5s^25p^64f^{12}n\ell$ . In the relativistic configuration interaction (RCI) procedure, the Dirac-Coulomb-Breit Hamiltonian with the addition of quantum electrodynamics (QED) terms such as the self-energy (SE) and vacuum polarization (VP) interactions has been diagonalized on the 3 545 069 CSFs basis in order to determine the corresponding eigenvalues and eigenvectors.

## The Ab initio MCDHF Method

## MCDHF-RCI-B

We have followed a different strategy in this second *ab initio* calculation. More specifically, the same MR as in our MCDHF-RCI-A calculation was retained, but the AS was here 7s6p7d5f with one correlation shell per  $\ell$  symmetry, and a different optimization scheme was chosen. It was carried out in three steps. In the first step, the core orbitals along with the 5s, 5p and 4f orbitals were optimized on the ground configuration using an EAL procedure similar to our preceding *ab initio* calculation. The second step consisted of a MCDHF Extended Optimize Level (EOL) [8] SCF optimization of all the other spectroscopic orbitals, namely 6s, 5d and 6d, on all the 333 levels of the MR keeping the orbitals of the previous step frozen. In the last step, the CSFs basis was extended to 3 261 592 CSFs by considering all the single and double excitations from the occupied 5s, 5p, 5d, 6s, 6d and 4f orbitals to the AS and by keeping only the CSFs that interact significantly with the 333 CSFs of the MR through the DCB hamiltonian. The correlation orbitals, *i.e.* 7s, 6p, 7d and 5f, were then optimized on the 333 levels of the MR during a MCHDF EOL SCF procedure. Finally, a RCI calculation was carried out on the 3 261 592 CSFs basis where the QED interactions were added to the DCB hamiltonian.

# RESULTS

20

In Table 1, our three sets of computed level energies, namely HFR, MCDHF-RCI-A and MCDHF-RCI-B, are compared to the experimental values of Ryabtsev *et al.* [5]. For the purpose of conciseness as we focus on the transition rates, the many unobserved even-parity levels that are located between the observed ones are not shown. Also reported in this table are the *LS*-coupling compositions as computed in our HFR model showing the first three major components. As one can see, most of the levels are strongly mixed with a purity less or equal to 50 %. For the purpose of clarity, we have plotted in Figures 1–3 **the** difference between the level energy calculated in our three independent models and the one determined experimentally by Ryabtsev *et al.* [5] as function of the latter.

# RESULTS

21

The root mean squares (RMS) of these differences were respectively:  $423 \text{ cm}^{-1}$  for our HFR model (Figure 1);  $10\,392 \text{ cm}^{-1}$  for our MCDHF-RCI-A model (Figure 2);  $6\,977 \text{ cm}^{-1}$  for our MCDHF-RCI-B model (Figure 3). As expected, our semi-empirical HFR model reproduces the experimental energy spectrum better, as it was fitted to minimize these energy differences. Regarding our *ab initio* calculations, one can also clearly notice that our MCDHF-RCI-B level energies reproduce the experiment much better than our MCDHF-RCI-A model, probably due to a better representation of the correlation effects through a more adequate choice of orbitals, meaning the use of correlation orbitals correcting the spectroscopic ones.

## RESULTS

22

## a sample, a part of our levels table

**Table:** Comparison between the present calculated and the available experimental energy levels in Hf VI.

$i$	$E_{exp}^a$ ( $\text{cm}^{-1}$ )	$E_{HFR}^b$ ( $\text{cm}^{-1}$ )	$E_{RCI-A}^c$ ( $\text{cm}^{-1}$ )	$E_{RCI-B}^d$ ( $\text{cm}^{-1}$ )	$J$	LS Composition <sup>e</sup>
1	0	0	0	0	7/2	100% $4f^{13} 2F^o$
2	13513.6	13514	13292	13270	5/2	100% $4f^{13} 2F^o$
3	97710	97710	132600	123123	3/2	100% $5p^5 4f^{14} 2P^o$
4	162465	162465	197296	188295	1/2	100% $5p^5 4f^{14} 2P^o$
5	224555	224849	227338	222833	7/2	36% $4f^{12} 5d ({}^3H)^4F$ + 21% $4f^{12} 5d ({}^3F)^4F$ + 10% $4f^{12} 5d ({}^4F)^4D$
6	229066	229272	232783	228471	9/2	25% $4f^{12} 5d ({}^3F)^4G$ + 15% $4f^{12} 5d ({}^3F)^2G$ + 15% $4f^{12} 5d ({}^1G)^2H$
7	230797	230878	234091	229598	7/2	34% $4f^{12} 5d ({}^3H)^4F$ + 17% $4f^{12} 5d ({}^3H)^4G$ + 16% $4f^{12} 5d ({}^3F)^4D$
8	231679	232150	235312	230753	9/2	44% $4f^{12} 5d ({}^3H)^4G$ + 15% $4f^{12} 5d ({}^3F)^4F$ + 13% $4f^{12} 5d ({}^3H)^4H$
9	234488	234658	238214	233524	7/2	62% $4f^{12} 5d ({}^3H)^2F$ + 10% $4f^{12} 5d ({}^3H)^4G$ + 8% $4f^{12} 5d ({}^3F)^4G$
10	238045	238129	242036	237383	7/2	31% $4f^{12} 5d ({}^3F)^4D$ + 19% $4f^{12} 5d ({}^1G)^2G$ + 8% $4f^{12} 5d ({}^3H)^4H$

# RESULTS

23

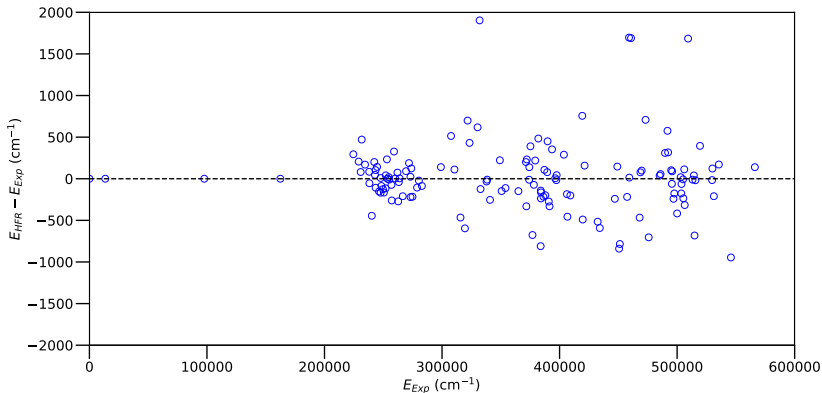


**Figure:** Comparison of HFR energy levels with respect to experiment. The energy difference is plotted versus the experimental energy. The root mean square of the differences is equal to 423 cm<sup>-1</sup>. Black dashed line: straight line of equality.

# RESULTS

24

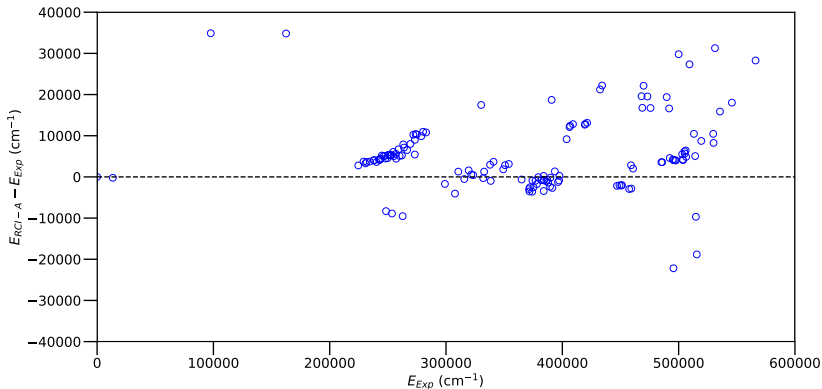


**Figure:** Comparison of MCDHF-RCI-A energy levels with respect to experiment [5]. The energy difference is plotted versus the experimental energy. The root mean square of the differences is equal to  $10\,392\text{ cm}^{-1}$ . Black dashed line: straight line of equality.



## RESULTS

25

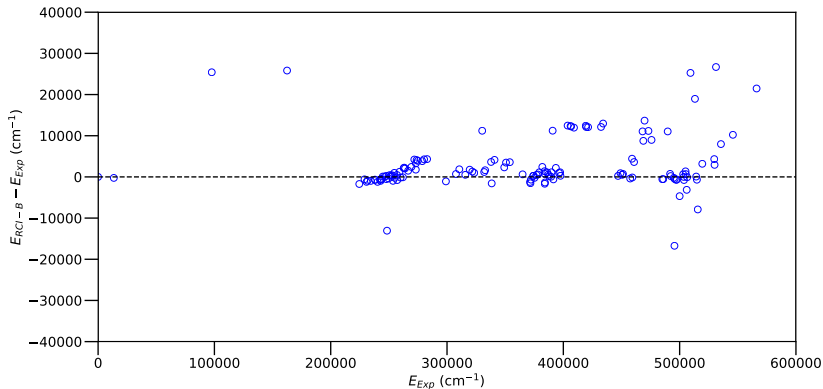


**Figure:** Comparison of MCDHF-RCI-B energy levels with respect to experiment [5]. The energy difference is plotted versus the experimental energy. The root mean square of the differences is equal to  $6\,977\text{ cm}^{-1}$ . Black dashed line: straight line of equality.

# RESULTS

26

The transition probabilities,  $gA$ , oscillator strengths in the logarithmic scale,  $\log gf$ , with their corresponding uncertainty indicators, namely the cancellation factor (CF) as defined by Cowan [7] for the HFR method and the uncertainty indicator  $dT$  as defined by Ekman *et al.* [10] for the MCDHF method, as computed in our three independent models are reported in Table 20 for the 185 E1 transitions observed in the spectral range  $193 \text{ \AA} < \lambda < 474 \text{ \AA}$  by Ryabtsev *et al.* [5]. Our *ab initio*  $gA$ - and  $\log gf$ -values, *i.e.* those computed in both our MCDHF models, have been rescaled using the experimental wavelengths [5]. The corresponding transition probabilities as calculated by Ryabtsev *et al.* [5] using the same HFR method but with more limited CI expansions are also presented for comparison. The latter **have** been used as reference **values** to deduce the uncertainty indicator (*Unc.* columns in Table 20) as defined by NIST [11] following the procedure described by Kramida [12].

# RESULTS

27

From that table, one notices that two relatively strong transitions predicted by Ryabtsev *et al.* [5], *i.e.* lines at 223.172 Å with  $gA_{RYA} = 6.13E + 10 \text{ s}^{-1}$  and at 231.451 Å with  $gA_{RYA} = 4.91E + 10 \text{ s}^{-1}$ , are affected by strong cancellation effects in our HFR model with CF of, respectively, 0.05 and 0.03, and corresponding  $gA_{HFR}$ -values of  $5.13E+08$  and  $1.59E+07 \text{ s}^{-1}$ . In Figure 4, a comparison of our HFR transition probabilities,  $gA_{HFR}$ , with respect to the calculation of Ryabtsev *et al.* [5],  $gA_{RYA}$ , is shown. The ratio,  $gA_{HFR}/gA_{RYA}$ , is plotted versus our HFR line strength,  $S_{HFR}$ , both in logarithmic scale. Similar plots are displayed for our MCDHF-RCI-A model in Figure 5 and for our MCDHF-RCI-B model in Figure 6. In these three figures, one can see that a large scatter of up to several orders of magnitudes occurs for the weak transitions, *i.e.* having a small line strength (typically  $S < 1$  a.u.). Most of these discrepancies can be explained by the fact that the majority of these transitions are affected by strong cancellation effects (with  $CF < 0.05$ ) that render weak lines even weaker [7] or by a strong gauge disagreement (with  $dT > 0.1$ ). They both indicate a strong model sensitivity.

# RESULTS

28

Concerning the strongest transitions (with  $S \geq 1$  a.u.), the average ratio of our transition probabilities with respect to the values calculated by Ryabtsev *et al.* [5], used as reference, is equal to 0.97 with a standard deviation of 0.08 for our HFR model, to 0.93 with a standard deviation of 0.41 for our MCDHF-RCI-A model, and to 0.81 with a standard deviation of 0.26 for our MCDHF-RCI-B model. First, it denotes a better agreement (by a few percent) between both HFR models. Second, although both our MCDHF models produce systematically lower rates (by  $\sim 10\%$  for MCDHF-RCI-A and by  $\sim 20\%$  for MCDHF-RCI-B) than in both HFR models, the strategy adopted in our MCDHF-RCI-B model improves the accord with the latter as the standard deviation of the ratios has reduced by a half.

## RESULTS

29

Table 3 (continued)

$\lambda^a$ (Å)	$i^b$	$k^b$	HFR <sup>c</sup>				RCI-A <sup>d</sup>				RCI-B <sup>e</sup>				RYA <sup>f</sup>
			$gA$ (s <sup>-1</sup> )	$\log gf$	$CF^g$	$Unc.^h$	$gA^i$ (s <sup>-1</sup> )	$\log gf^i$	$dT^j$	$Unc.^h$	$gA^i$ (s <sup>-1</sup> )	$\log gf^i$	$dT^j$	$Unc.^h$	$gA$ (s <sup>-1</sup> )
389.138	1	30	2.57E+09	-1.23	0.04	E	2.03E+09	-1.34	0.17	E	2.65E+09	-1.22	0.32	E	1.19E+09
390.818	2	39	5.38E+08	-1.91	0.03	E	2.62E+08	-2.22	0.01	E	1.63E+08	-2.43	0.14	E	4.00E+08
392.069	1	29	8.85E+08	-1.69	0.08	E	2.56E+08	-2.23	0.08	E	2.68E+08	-2.21	0.32	E	3.60E+08
392.664	1	28	3.97E+09	-1.04	0.06	F	1.84E+09	-1.37	0.09	F	1.79E+09	-1.38	0.14	F	1.63E+09
452.543	2	9	1.51E+08	-2.33	0.02	E	9.60E+07	-2.53	0.09	E	9.02E+07	-2.56	0.36	E	8.00E+07
473.842	2	5	4.45E+07	-2.83	0.01	E	2.53E+07	-3.07	0.02	E	2.03E+07	-3.17	0.29	E	2.00E+07

<sup>a</sup> Experimental values from Ryabtsev et al. [5];

<sup>b</sup> Lower and upper level indices, respectively  $i$  and  $k$ , given in the first column of Table 2.

<sup>c</sup> Our HFR calculation;

<sup>d</sup> Our MCDHF-RCI-A calculation;

<sup>e</sup> Our MCDHF-RCI-B calculation;

<sup>f</sup> Hartree-Fock calculation of Ryabtsev et al. [5];

<sup>g</sup> Cancellation factor as defined in Cowan [7];

<sup>h</sup> Uncertainty indicator as defined by NIST [11], here  $C+ \leq 18\%$ ,  $C \leq 25\%$ ,  $D+ \leq 40\%$ ,  $D \leq 50\%$ ,  $E > 50\%$ , evaluated with respect to the  $gA$ -values of Ryabtsev et al. [5] using the methodology described by Kramida [12];

<sup>i</sup> Given in the Babushkin gauge;

<sup>j</sup> Uncertainty indicator as defined in Ekman et al. [10];

<sup>k</sup> Doubly classified in Ryabtsev et al. [5].

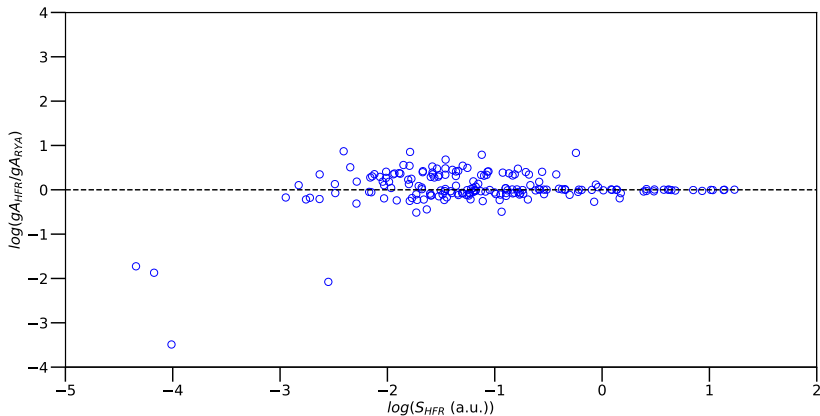


**Figure:** Comparison of our HFR transition probabilities,  $gA_{HFR}$ , with respect to the values calculated by Ryabtsev *et al.* [5],  $gA_{RYA}$ . The ratio,  $gA_{HFR}/gA_{RYA}$ , is plotted versus our HFR line strength,  $S_{HFR}$ , both in logarithmic scale. Black dashed line: straight line of equality. The average and the standard deviation of the ratios is respectively equal to 0.97 and 0.08 for a sample restricted to the strongest lines, *i. e.*  $S_{HFR} \geq 1$  a.u. This plot is used to evaluate the uncertainty indicator as defined in NIST [11] on our HFR rates following the procedure described by Kramida [12].

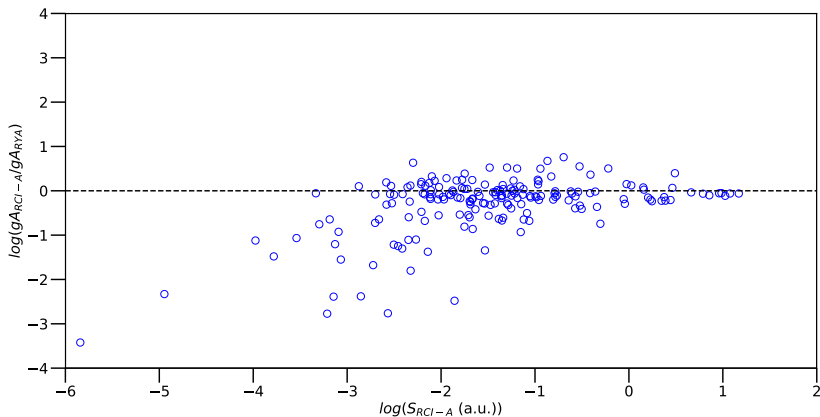


**Figure:** Comparison of our MCDHF-RCI-A transition probabilities corrected with the experimental wavelengths [5],  $gA_{RCI-A}$ , with respect to the values calculated by Ryabtsev *et al.* [5],  $gA_{RYA}$ . The ratio,  $gA_{RCI-A} / gA_{RYA}$ , is plotted versus our RCI-A line strength,  $S_{RCI-A}$ , both in logarithmic scale. Black dashed line: straight line of equality. The average and the standard deviation of the ratios is respectively equal to 0.93 and 0.41 for a sample restricted to the strongest lines, *i.e.*  $S_{RCI-A} \geq 1$  a.u.

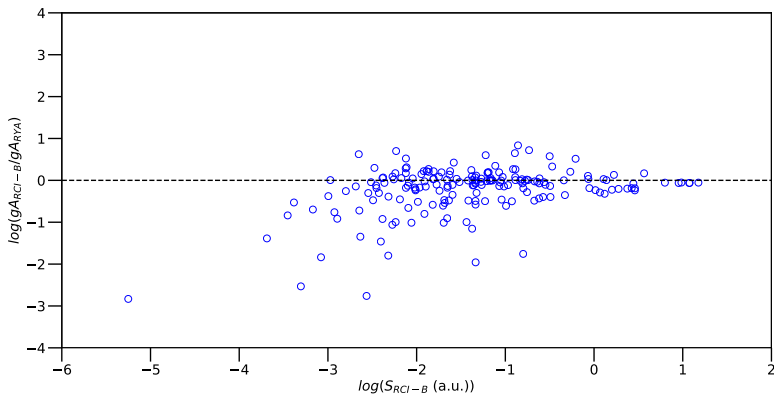


**Figure:** Comparison of our MCDHF-RCI-B transition probabilities corrected with the experimental wavelengths [5],  $gA_{RCI-B}$ , with respect to the values calculated by Ryabtsev *et al.* [5],  $gA_{RYA}$ . The ratio,  $gA_{RCI-B} / gA_{RYA}$ , is plotted versus our RCI-B line strength,  $S_{RCI-B}$ , both in logarithmic scale. Black dashed line: straight line of equality. The average and the standard deviation of the ratios is respectively equal to 0.81 and 0.26 for a sample restricted to the strongest lines, *i.e.*  $S_{RCI-B} \geq 1$  a.u. This plot is used to evaluate the uncertainty indicator as defined in NIST [11] on our MCDHF-RCI-B rates following the procedure described by Kramida [12].



# Conclusion

33

The Hf VI radiative parameters have been calculated for the 185 E1 transitions observed by Ryabtsev *et al.* [5] in the UV range from 193 Å to 474 Å. As no experimental determination of radiative rates is available in the literature, a multiplatform approach has been adopted to carry out the present calculations so as to estimate the accuracy of the computed rates. From the comparisons of our three independent models based on both the HFR [7] and MCDHF [9, 8] methods along with the calculations published by Ryabtsev *et al.* [5] that they used for line classification purpose, it was found that the uncertainties affecting the theoretical rates range from a few percent (for our HFR model) to  $\sim 40\%$  (for our MCDHF-RCI-A model) for the strong E1 transitions with  $S \geq 1$  a.u.

# Conclusion

34

With respect to the other lines, they can be highly inaccurate with uncertainties far more than 100 % due to strong cancellation effects and important gauge disagreements that render the rates highly model sensitive. This is essentially caused by the strong mixing affecting most of the Hf VI atomic states. Finally, we recommend our HFR rates except for the two lines at 223.172 Å and at 231.451 Å where the  $gA$ -values of Ryabtsev *et al.* [5] should be used instead with an uncertainty indicator *Unc.* equal to E (> 50 %), due to strong cancellation effects affecting the former for these two transitions.





# Conclusion






35




This work was published in Journal of Quantitative Spectroscopy and Radiative Transfer

<https://doi.org/10.1016/j.jqsrt.2023.108529>

PQ and PP are respectively Research Director and Research Associate of the Belgian Fund for Scientific Research F.R.S.-FNRS. Financial support from this organization is gratefully acknowledged. EBM is grateful to Belgian colleagues for their hospitality during his stay at Université de Mons - UMONS. EBM and SEY were supported by Marien Ngouabi University from Congo.

-  Linsmeier C, Rieth M, Aktaa J, Chikada T, Hoffmann A, Houdou A, Kurishita H, Jin X, Li M, Litnovsky A, Matsuo S, von Müller A, Nikolic V, Palacios T, Rippan R, Qu S, Reiser J, Riesch J, Shikama T, Stieglitz R, Weber T, Wurster S, You J-H, Zhou Z. Development of advanced high heat flux and plasma-facing materials. Nucl Fusion 2017;57:092007. doi:10.1088/1741-4326/aa6f71.
-  Pillon M, Angelone M, Forrest R A. Measurements of fusion-induced decay heat in materials and comparison with code predictions. Radiat Phys Chem 2004;71:895. doi:10.1016/j.radphyschem.2004.04.119.
-  Gilbert M R, Sublet J-C. Neutron-induced transmutation effects in W and W-alloys in a fusion environment. Nucl Fusion 2011;51:043005. doi:10.1088/0029-5515/51/4/043005.
-  Ryabtsev A N, Kononov E Ya, Kildiyarova R R, Tchang-Brillet W-Ü L, Wyart J-F.  $4f^{13}5s^25p^6 - 4f^{13}5s^25p^56s$  Transitions in the W VIII Spectrum and Spectra of Isoelectronic Hafnium, Tantalum, and Rhenium Ions. Opt Spectrosc 2012;113:109. doi:10.1134/S0030400X12080140.

-  Ryabtsev A N, Kononov E Ya, Kildiyarova R R, Tchang-Brillet W-Ü L, Wyart J-F, Champion N, Blaess C. Spectra of the W VIII isoelectronic sequence: I. Hf VI. Phys Scr 2014;89:115402. doi:10.1088/0031-8949/89/11/115402.
-  Bokamba Motoumba E, Enzonga Yoca S, Quinet P, Palmeri P. Calculations of transition rates in erbium-like ions Lu IV, Hf V and Ta VI using the Ab initio MCDHF-RCI and semi-empirical HFR methods. ADNDT 2020;133-134:101340.
-  Cowan RD. The Theory of Atomic Structure and Spectra. Berkeley: University of California Press; 1981.
-  Froese Fischer C, Gaigalas G, Jönsson P, Bieroń J, Grant IP. GRASP2018-A Fortran 95 version of the General Relativistic Atomic Structure Package. Comput Phys Commun 2019;237:184.
-  Grant IP. Relativistic quantum theory of atoms and molecules. Theory and computation. New York: Springer; 2007.

-  Ekman J, Godefroid M, Hartman H. Validation and implementation of uncertainty estimates of calculated transition rates. *Atoms* 2014;2:215.
-  Kramida A, Ralchenko Yu, Reader J, and NIST ASD Team (2022). NIST Atomic Spectra Database (ver. 5.10), [Online]. Available: <https://physics.nist.gov/asd> [2023, January 18]. National Institute of Standards and Technology, Gaithersburg, MD. DOI: <https://doi.org/10.18434/T4W30F>.
-  Kramida A. Critical evaluation of data on atomic energy levels, wavelengths, and transition probabilities. *Fusion Science and Technology* 2013;63:313.

Thanks for your attention!